ADVANCES IN ATMOSPHERIC SCIENCES, VOL. 30, NO. 1, 2013, 89–100

The Application of Flux-Form Semi-Lagrangian Transport Scheme in a Spectral Atmosphere Model

WANG Xiaocong[1,2] (王晓聪), LIU Yimin*[1] (刘屹岷), WU Guoxiong[1] (吴国雄), Shian-Jiann LIN[3], and BAO Qing[1] (包 庆)

[1] *State Key Laboratory of Numerical Modeling for Atmospheric Sciences and Geophysical Fluid Dynamics, Institute of Atmospheric Physics, Chinese Academy of Sciences, Beijing* 100029

[2] *University of Chinese Academy of Sciences, Beijing* 100049

[3] *NOAA/Geophysical Fluid Dynamics Laboratory, Princeton University, Princeton, New Jersey*

(Received 22 February 2012; revised 8 April 2012)

ABSTRACT

A flux-form semi-Lagrangian transport scheme (FFSL) was implemented in a spectral atmospheric GCM developed and used at IAP/LASG. Idealized numerical experiments show that the scheme is good at shape preserving with less dissipation and dispersion, in comparison with other conventional schemes. Importantly, FFSL can automatically maintain the positive definition of the transported tracers, which was an underlying problem in the previous spectral composite method (SCM). To comprehensively investigate the impact of FFSL on GCM results, we conducted sensitive experiments. Three main improvements resulted: first, rainfall simulation in both distribution and intensity was notably improved, which led to an improvement in precipitation frequency. Second, the dry bias in the lower troposphere was significantly reduced compared with SCM simulations. Third, according to the Taylor diagram, the FFSL scheme yields simulations that are superior to those using the SCM: a higher correlation between model output and observation data was achieved with the FFSL scheme, especially for humidity in lower troposphere. However, the moist bias in the middle and upper troposphere was more pronounced with the FFSL scheme. This bias led to an over-simulation of precipitable water in comparison with reanalysis data. Possible explanations, as well as solutions, are discussed herein.

Key words: advection, precipitation, spectral composite method, flux-form semi-Lagrangian, Spectral Atmospheric Model of the IAP/LASG (SAMIL)

Citation: Wang, X. C., Y. M. Liu, G. X. Wu, S. J. Lin, and Q. Bao, 2013: The application of flux-form semi-Lagrangian transport scheme in a spectral atmosphere model. *Adv. Atmos. Sci.*, **30**(1), 89–100, doi: 10.1007/s00376-012-2039-2.

1. Introduction

The advection process is of vital importance in fluid dynamics. The properties of an advection scheme are pivotal to proper representation of fluid dynamical phenomena in numerical models. In atmospheric science, advection modeling is most closely associated with the solution of motion equations as well as the constituent continuity equation. Thus far, many approaches to the advection equation in atmospheric science have been put forward. The canonical finite difference method (FDM) has been widely used during the past several decades. However, a common underlying problem of the FDM is the fact that discrete numerical approaches inevitably introduce dispersion and dissipation into the approximate solution. In addition, due to polar singularity, the models inevitably suffer from the rigid limitation of the Courant–Friedrich–Lev (CFL) number, as well as large computational errors, when FDM is used. The spectral composite method (SCM) is another important approach in the solution of advection equations, especially for spectral models. For a smooth field, the SCM can significantly improve the accuracy of advec-

*Corresponding author: LIU Yimin, lym@lasg.iap.ac.cn

tion modeling because the high-order spatial algorithm is built in. However, the Gibbs phenomenon becomes a potential problem when SCM is used for the advection of water species, namely cloud water or cloud ice, because these water species are usually discontinuous in the real atmosphere. Additionally, the definitive properties of tracers cannot be guaranteed by SCM. These deficiencies in FDM and SCM, respectively, led to the development of the semi-Lagrangian method (SLM), which has received great attention since the pioneering work of Nielsen (1959). In addition to its high accuracy in numerical dispersion (McDonald, 1984, 1987; Ritchie, 1985, 1987; Rood, 1987), the advantage of SLM is its adaptation to large Courant numbers. In the work of Robert (1981, 1982), stable integrations were successful when SLM was used, even with the time interval up to two hours. A further study demonstrated that the time step could be four to six times as large as the maximum permitted for an equivalent Eulerian method. Staniforth and Côté (1991) gave a detailed review of this method and its applications to atmospheric modeling. For scalar transport, monotonic upstream-biased transport schemes have received much attention, as the positive definition of the transported constituent is automatically maintained. In general, the application of any of the following schemes is very successful: unidimensional (1D, hereafter) monotonic schemes such as Smolarkiewicz's scheme (Smolarkiewicz and Grabowski, 1990), van Leer's scheme (van Leer, 1977, 1979) and its variant, the piece-wise parabolic method (PPM, Colella and Woodward, 1984), and the piece-wise rational method (PRM, Xiao and Peng, 2004). When extending a 1D scheme to greater dimensions, the operator splitting technique is usually used. However, the splitting process, which replaces a complex problem with a series of simple problems, often introduces errors, which can lead to the failure of multidimensional applications. To effectively eliminate errors introduced by the splitting process, Lin and Rood (1996) developed a multidimensional flux-form semi-Lagrangian (FFSL) transport scheme that reduces the dimensionality of the physical problem from three dimensions to two dimensions using the concept of vertically Lagrangian discretization (Lin, 2004). In addition, properties such as conservation and consistency are well considered in FFSL scheme. Due to its advantages, the FFSL scheme is now widely used in many GCMs, namely NASA Goddard Institute for Space Studies (GISS) GCM, Geophysical Fluid Dynamics Laboratory (GFDL) Atmosphere Model (AM), and Max Planck Institute (MPI) European Center/Hamburg Model (ECHAM) (Roeckner et al., 2003).

A Spectral Atmospheric Model of the Institute of Atmospheric Physics (IAP)/State key Laboratory of Numerical Modeling for Atmospheric Physics and Geophysical Fluid Dynamics (LASG) (SAMIL) has been developed and used at IAP/LASG since the 1990s (Wu et al., 1996, 2004; Wang et al., 2005a, b; Bao et al., 2006). In SAMIL, moisture advection is calculated using the SCM. As described above, the SCM cannot guarantee conservation and/or consistency of water vapor and easily yields negative values. Furthermore, this method poses serious disadvantages when more discontinuous substances, such as cloud water or cloud ice, are introduced. Therefore, a mass conservation method for the advection process is necessary to further develop SAMIL.

In this study, the FFSL scheme was implemented in SAMIL, and its performance was first examined using a standard test case for the advection of the cosine-bell function over the pole, which is usually used for testing numerical approximations in spherical geometry (Williamson et al., 1992). Results were verified by numerical experiments and were then analyzed in comparison with SCM results. This paper has been divided into the following sections: In section 2, we describe the main algorithm of FFSL, as well as the 1D PPM scheme, a higher-order van Leer type scheme employed in FFSL. In section 3, we provide a brief description of the SAMIL model, and we report the performance of the modified SAMIL using FFSL as well as the previous version. The respective results were analyzed and compared to interpret the impact of the FFSL scheme on GCM results. And finally, in section 4 discussion of the results and conclusions of the study are presented.

2. Multidimensional FFSL transport scheme

2.1 *1D advection scheme: PPM*

In this section, the PPM scheme for solving a linear advection equation is briefly described. The 1D advection equation can be written as

$$\frac{\partial f}{\partial t} + u\frac{\partial f}{\partial x} = 0 \,, \tag{2.1}$$

where f represents any transported scalar, while u, t, x stands for zonal wind, time, distance in horizontal dimension, respectively. From the Lagrangian view, the scalar f at time t_{n+1} is solved as

$$f(x, t_{n+1}) = f(x - u\Delta t, t_n) \,. \tag{2.2}$$

Accordingly, the discrete form is written as

$$f(x_j, t_{n+1}) = \frac{1}{\Delta x_j}\int_{x_{j-1/2}}^{x_{j+1/2}} f(x - u\Delta t, t_n)dx \,, \tag{2.3}$$

where j is the index of the point in horizontal dimension. Δt, Δx stands for time and distance interval, respectively. $x_{j+1/2}$ is the boundary between the jth and the $(j+1)$th zones on the computational grid. The representative form of f, also named the interpolation polynomial, determines the overall accuracy of the algorithm. Different from the traditional upstream scheme, which assumes a mean value inside the cell, the PPM scheme uses a piecewise parabolic interpolation (Colella and Woodward, 1984):

$$f(x) = f_{\mathrm{L},j} + y[f_{\mathrm{R},j} - f_{\mathrm{L},j} + f_{6,j}(1-y)]\,, \tag{2.4}$$

$$y = \frac{x - x_{j-1/2}}{\Delta x_j}\,,\quad x_{j-1/2} \leqslant x \leqslant x_{j+1/2}\,, \tag{2.5}$$

$$f_{6,j} = 6\left[f_j - \frac{1}{2}(f_{\mathrm{L},j} + f_{\mathrm{R},j})\right]\,, \tag{2.6}$$

where the interface value $f_{\mathrm{L},j}$, $f_{\mathrm{R},j}$ is the left and right boundary value of f at x_j. They both are calculated using a high-order interpolation from nearby zones. Alternatively, the cell-bound value can also be calculated using a semi-Lagrangian procedure (Xiao et al., 2002). Finally, we can express the calculation of $f_{j,n+1}$ in explicit conservation form:

$$f_{j,n+1} = f_{j,n} - u\frac{\Delta t}{\Delta x}\left[f_{\mathrm{a},j+\frac{1}{2},\mathrm{L}}(u\Delta t) - f_{\mathrm{a},j-\frac{1}{2},\mathrm{L}}(u\Delta t)\right]\,,\quad u \geqslant 0 \tag{2.7}$$

$$f_{j,n+1} = f_{j,n} - u\frac{\Delta t}{\Delta x}\left[f_{\mathrm{a},j+\frac{1}{2},\mathrm{R}}(-u\Delta t) - f_{\mathrm{a},j-\frac{1}{2},\mathrm{R}}(-u\Delta t)\right]\,,\quad u \leqslant 0 \tag{2.8}$$

where f_{a} is the average of the interval.

With regard to the performance of the PPM scheme, an idealized test of square-wave advection (CFL=0.5) was conducted, along with tests of the other three conventional transport schemes. Figure 1 shows the wave status at step 500 and step 800. The upstream scheme exhibited a clear dissipation near the sharp gradient (Fig. 1a), while the Lax-Wendroff

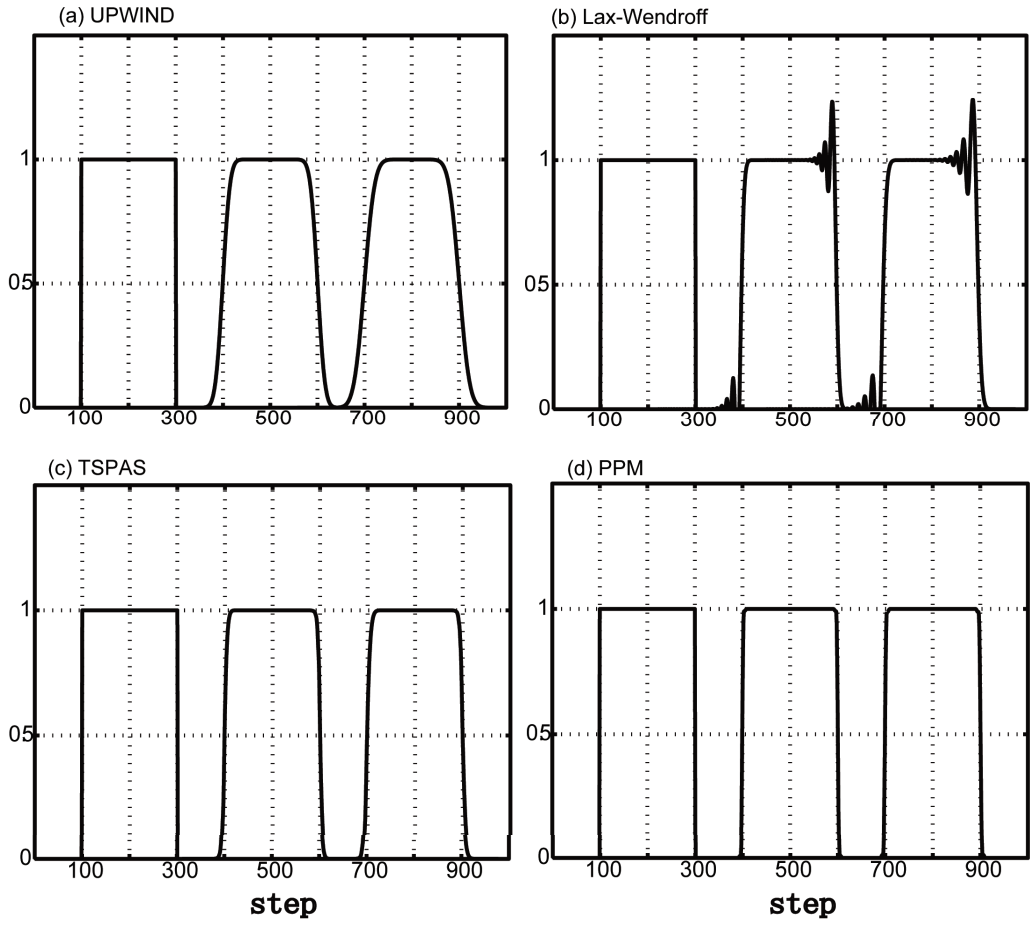

Fig. 1. Performance of idealized 1D square-wave advection test (CFL=0.5) using the following schemes: (a) UPSTREAM, (b) Lax-Wendroff, (c) TSPAS, and (d) PPM. The ordinate stands for the impulse of square-wave.

scheme exhibited obvious oscillation in steeper discontinuities (Fig. 1b). However, the second-order Lax-Wendroff scheme was more accurate than the first-order upstream scheme: less dissipation was produced. Nevertheless, the merit of the nonoscillatory pattern of the upstream scheme is also notable. Combining these ideas, Yu (1994) proposed a new two-step nonoscillatory shape-preserving, positive-definition, finite-difference advection scheme (TSPAS), which merged the advantages of small dispersion error of the simple first-order upstream scheme with small dissipation error of the simple second-order Lax-Wendroff scheme. The TSPAS shows a significant improvement in both dispersion and dissipation (Fig. 1c), although numerical errors still exist near the discontinuities. Compared with TSAPS, the PPM simulation (Fig. 1d) had the highest accuracy in the steeper discontinuities, as the square-wave shape was well preserved after advection. Furthermore, the PPM scheme can be easily extended to large time steps due to the immunity of the CFL constraint of the Lagrangian algorithm.

2.2 *Extension to multiple dimensions*

While PPM possesses all the desirable attributes (mass conserving, monotonicity preserving, and high-order accuracy) of 1D advection, for multidimensional modeling, the errors caused by directional splitting should be avoided. Fortunately, Lin and Rood (1996) resolved these errors by applying the two orthogonal 1D flux-form operators in a symmetric way. At the same time, the "inner operators" are replaced with advective-form operators to create consistency. The mathematical form is written as follows (Lin and Rood, 1996):

$$
\begin{aligned}
Q_{n+1} &= \frac{1}{2}(Q_{xy} + Q_{yx}) \\
&= Q_n + F(Q_n) + G(Q_n) + \\
&\quad \frac{1}{2}[GF(Q_n) + FG(Q_n)] \qquad (2.9) \\
&= Q_n + F\left[Q_n + \frac{1}{2}G(Q_n)\right] + \\
&\quad G\left[Q_n + \frac{1}{2}F(Q_n)\right] \qquad (2.10) \\
&= Q_n + F\left[Q_n + \frac{1}{2}g(v_{\mathrm{a}}^*, \Delta t; Q_n)\right] + \\
&\quad G\left[Q_n + \frac{1}{2}f(u_{\mathrm{a}}^*, \Delta t; Q_n)\right] \qquad (2.11)
\end{aligned}
$$

where outer operators F and G are in flux form, while inner operators f and g are in advective form, and $(u_{\mathrm{a}}^*, v_{\mathrm{a}}^*)$ represent time-averaged winds. The subscript xy or yx stands for the transport sequence in horizontal direction. Finally, an accurate and conservative algorithm is used to remap the deformed Lagrangian coordinate back to a fixed Eulerian coordinate with the concept of Lagrangian control volume.

The general performance of the FFSL scheme was examined using an idealized over-polar advection experiment. As shown in Fig. 2, the cosine-bell function was accurately advected over the pole; the shape is less deformed. Although small dissipation occurs in the innermost circle, the performance is encouraging and acceptable for GCMs.

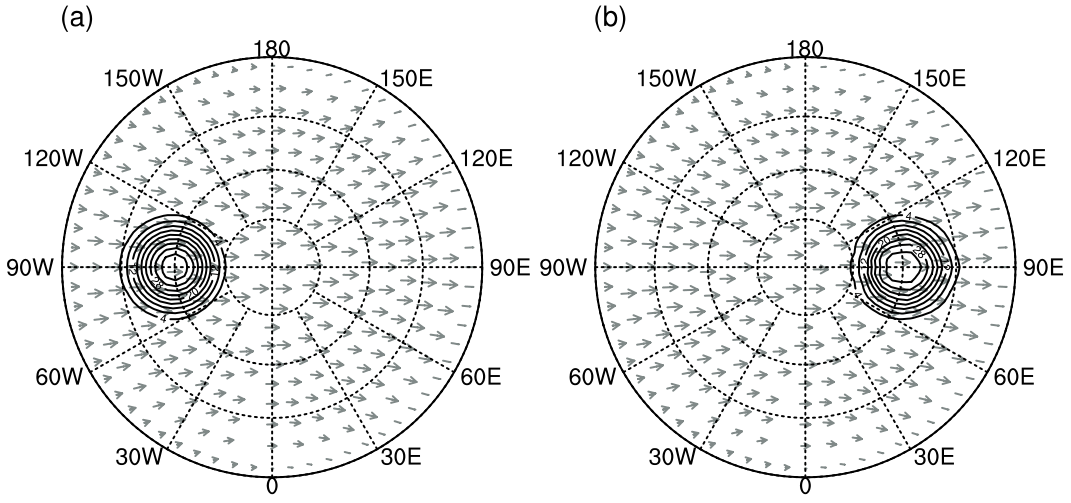

Fig. 2. Performance of advection of the cosine-bell function over the pole with the FFSL scheme: (a) initial state and (b) state after over-pole advection. (Units: g kg^{-1})

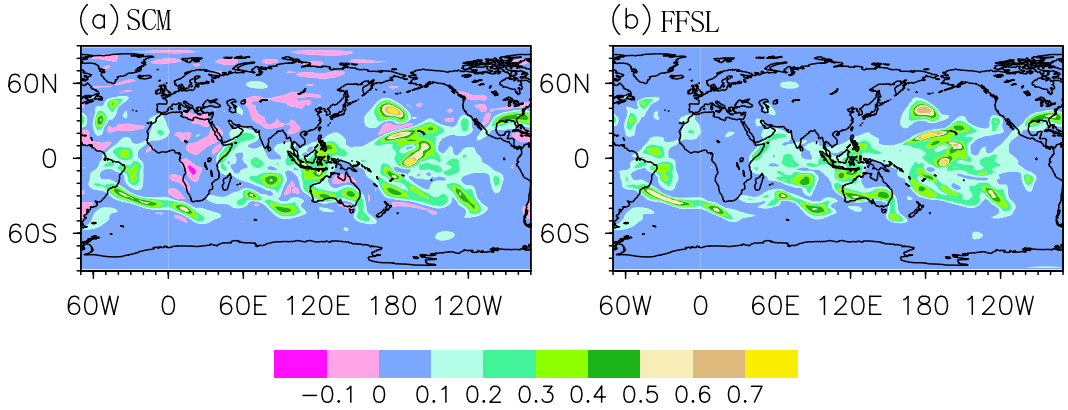

Fig. 3. Horizontal distribution of water vapor after 10-day advection by the two transport schemes: (a) SCM and (b) FFSL. (Units: g kg^{-1})

To visually highlight the advantages of the FFSL scheme, a 10-day integration of the dry model in which water vapor is merely taken as a passive tracer without any phase changes was conducted using two different transport schemes. Figure 3 displays the vapor distribution result on day 10. As shown in Fig. 3a, negative vapor was widely distributed in the SCM simulation, especially in arid continent regions, such as South Africa and the Tibetan Plateau. In the FFSL simulation (Fig. 3b), the spatial distribution of water vapor was very similar to that of the SCM simulation, but negative vapor were successfully suppressed.

3. Performance of FFSL in SAMIL

In this study, the FFSL scheme was implemented in a spectral AGCM for passive tracer transport only (e.g., water vapor), and its performance was compared with the previous SCM scheme as well as a series of reanalysis datasets. With regard to model implementation, the pivotal processes are summarized as follows. (1) velocity components for C-type grid staggering were prepared. (2) horizontal diffusions for water vapor were switched off when FFSL was used, due to the advantages of FFSL discussed in section 2. (3) a new parallelization strategy according to the FFSL scheme was designed, as the parallel compartmentalization with FFSL is totally different than that with the SCM scheme.

3.1 *Model description and datasets*

The model used in this study, SAMIL, is a spectral atmosphere model developed by IAP/LASG; it is an atmospheric component of the Flexible Global Ocean-Atmosphere-Land System (FGOALS) developed at LASG/IAP (Bao et al., 2010). The dynamical framework of this model is a hybrid-coordinate system with 26 vertical layers (L26), rhomboidally truncated at wave-number 42 in the horizontal (R42), providing a nominal Gaussian grid resolution of 2.8° (lon.) ×1.66° (lat.).Various grid and subgrid parameterization schemes are included in the physical package of SAMIL. The mass flux cumulus parameterization of Tiedtke (1989) is employed with the modification by Nordeng (1994), in which the closure for deep convection is based on CAPE rather than large-scale moisture convergence. This cumulus convection scheme works well in the simulation of MJO and ENSO (Liu et al., 2005), as the latent heating structure can be well represented (Song, 2005; Wang et al., 2011). The adjustment scheme by Manabe et al. (1995) is used for large-scale condensation. The radiation scheme is the Edwards–Slingo scheme from the UK Meteorological Office (Edwards and Slingo, 1996), but with a modification by Sun (2005). PBL parameterization of the model is a "non-local" scheme (Holtslag and Boville, 1993) that computes the turbulent transfer of momentum, heat, and moisture. The cloud scheme is a diagnostic method based on vertical motion and relative humidity (Slingo, 1980).

The model was integrated for 25 years under two advection schemes: SCM and FFSL. The average output of the last 10 years was used for analysis. The verification data used in this study consisted of (1) Global Precipitation Climatology Project (GPCP) analysis (Adler et al., 2003), (2) European Center for Medium-Range Weather Forecasts (ECMWF) 40 year reanalysis dataset (ERA40) (Uppala et al., 2005), and (3) National Centers for Environmental Prediction (NCEP)/National Center for Atmospheric Research (NCAR) reanalysis (Kalnay et al., 1996).

3.2 *Results*

3.2.1 *Precipitation*

Figure 4 shows the seasonal average precipitation of the last 10 years of model output, in comparison with the GPCP analysis. In winter, a well-

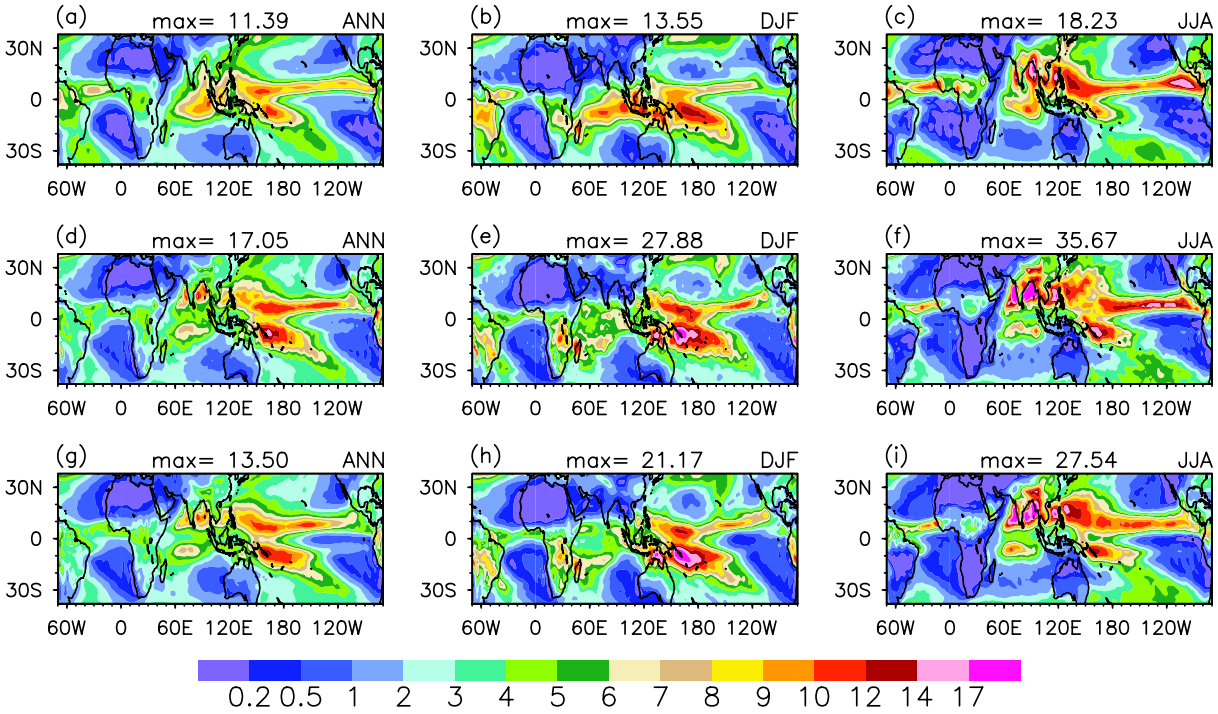

Fig. 4. Seasonal averages of tropical precipitation rate with GPCP reanalysis (a, b, c), SCM simulations (d, e, f), and FFSL simulations (g, h, i). (Units: mm d^{-1})

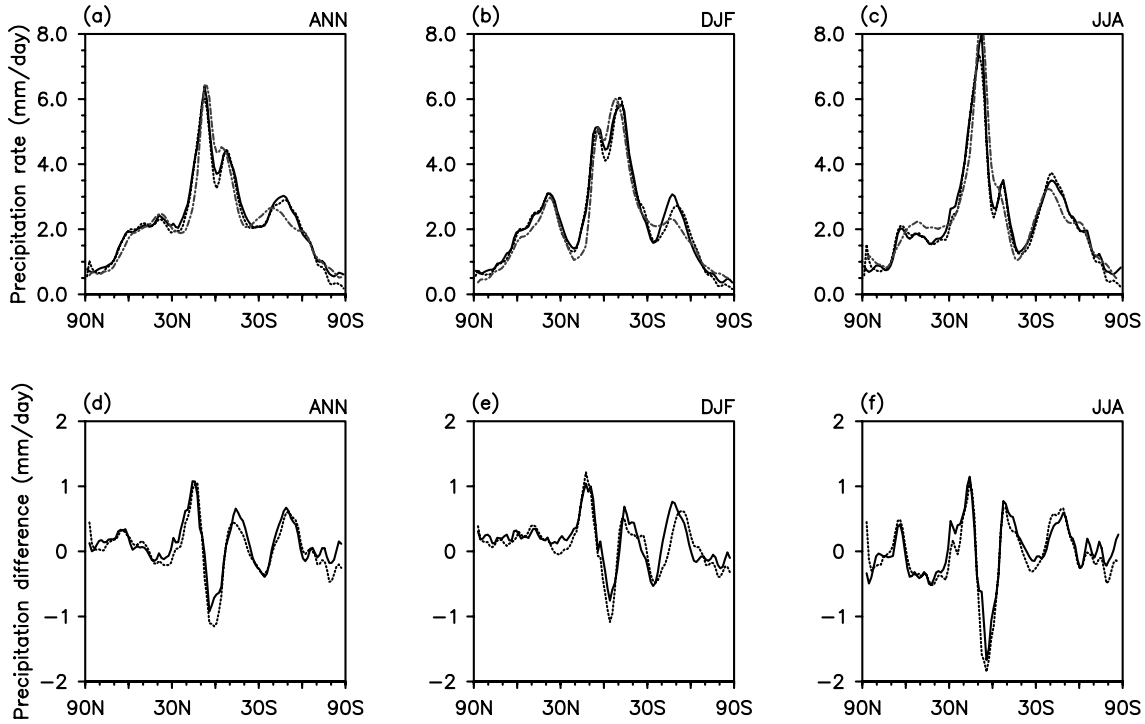

Fig. 5. Zonal mean precipitation rate (a, b, c) for SCM (solid line), FFSL (dotted line), GPCP (thick dash-dotted line), and the difference from GPCP reanalysis (d, e, f).

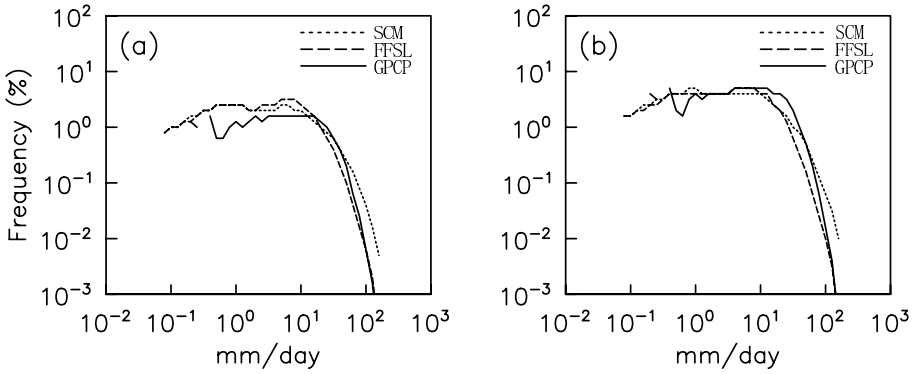

Fig. 6. Tropical precipitation frequency (35°S–35°N) obtained when (a) all samples were counted and (b) when only precipitation samples were counted. (Units: %)

distributed rain belt was located near and south of the equator (Fig. 4b), known as the southern Pacific convergence zone (SPCZ). The observed rainfall centers along and south of the equator were well captured in both schemes; they can be clearly seen in Figs. 4e and h. Although the simulated rainfall distributions by the two schemes were quite similar, the precipitation extremes were significantly different. The SCM scheme shows a maximum value of 27.88 mm d^{-1}; this value decreased to 21.17 mm d^{-1} with the FFSL scheme, which was closer to the GPCP reanalysis value (13.55 mm d^{-1}). The overestimated rainfall with the SCM scheme partly resulted from the advection process of water vapor, during which frequent transformation between spectral and Gaussian space caused non-negligible computing errors. Moreover, the artificial removal of negative water vapor was also responsible for the unrealistic simulation. For summer, the rain band shifts northward and the precipitation centers were located in the equatorial region, known as the ITCZ. According to GPCP analysis, a successive rain belt was located near the West Pacific warm pool, which was also well reproduced by FFSL scheme. However, a broken belt was located over 150°E (Fig. 4f), which was unreasonable in comparison with the GPCP analysis. In addition, the over-simulated maximum rainfall with the SCM scheme appeared again (Fig. 4f), reaching as high as 35.67 mm d^{-1}. With regard to annual mean, the simulated maximum rainfall by both schemes was greatly reduced, with 17.05 mm d^{-1} and 13.50 mm d^{-1}, respectively, which was close to the GPCP analysis value (11.39 mm d^{-1}). Overall, both rainfall distribution and intensity were significantly improved in the simulation with FFSL scheme. Figure 5 displays the observed and simulated zonal mean precipitation rates, along with their difference from GPCP reanalysis. Generally, the SAMIL model successfully reproduces rainfall variation across latitude with either transport scheme. The differences in rainfall variation with each scheme compared with GPCP reanalysis indicate that the precipitation was weakly reduced with the FFSL scheme compared to the SCM scheme (Figs. 5d–f).

The conspicuous difference in maximum rainfall inspired us to investigate the precipitation frequency (Fig. 6). The occurrence of heavy rain (>10 mm d^{-1}) was notably reduced with the FFSL scheme, which was consistent with the GPCP analysis. Additionally, the occurrence of moderate rain (between 1 mm d^{-1} and 10 mm d^{-1}) was overestimated by both schemes. This can be partly attributed to the imperfect cumulus convection and stratiform condensation schemes, as precipitation seems to form easily. Once the non-precipitation results were excluded, the re-obtained frequency of moderate precipitation was much closer to the GPCP reanalysis (Fig. 6b).

3.2.2 *Humidity, temperature and precipitable water*

The ERA40 reanalysis data for December–February (DJF) were compared to the simulated seasonal averages of zonal means of specific humidity, temperature, and relative humidity (Fig. 7). In Fig. 7a, a larger gradient of specific humidity occurred in the Northern Hemisphere. Because solar radiation directly irradiates the Southern Hemisphere in winter, temperature as well as water vapor varies gradually with latitude. As shown in Figs. 7d and g, both schemes well reproduced the observed distribution of water vapor, although deviations occurred. We noticed that both simulations show dry bias at lower levels and moist bias in upper levels, which is also reflected in other GCMs (Peng et al., 2005). However, the negative difference below 850 hPa was much stronger with the SCM scheme than with the FFSL scheme, indicating that the dry bias was significantly alleviated. Above the PBL, the FFSL scheme exhibited a stronger moist bias centering near the middle troposphere. This phe-

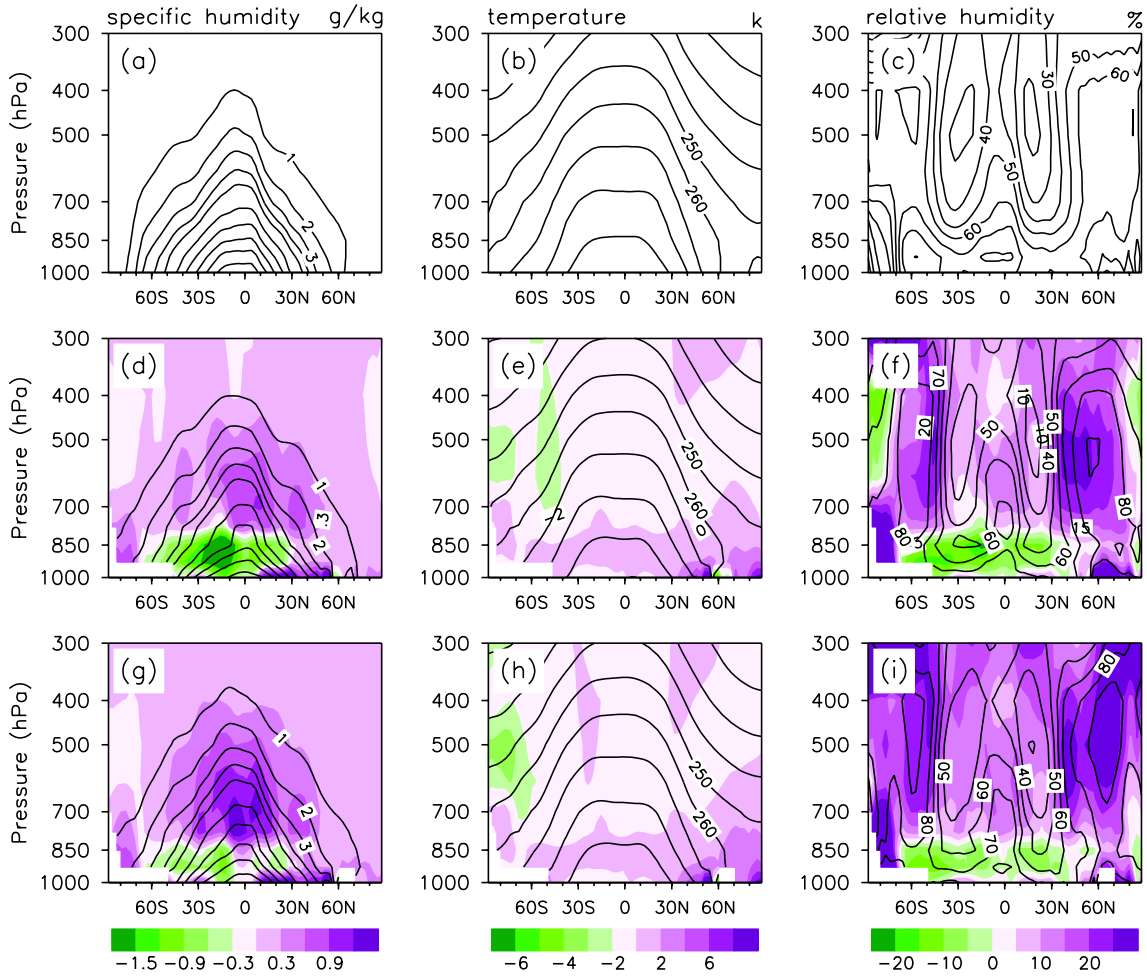

Fig. 7. December–February (DJF) averages of zonal average of specific humidity (a, d, g), temperature (b, e, h) and relative humidity (c, f, i) from ERA40 (a, b, c), SCM simulations (d, e, f), and FFSL simulations (g, h, i). Differences for simulation minus the ERA40 reanalysis (shaded) are also plotted in the corresponding panels.

nomenon does not imply that the FFSL scheme is inferior to the SCM scheme, although moist bias was indeed magnified in FFSL simulation. The most likely reason for this increase in bias is the imperfect representation of the water phase change above the PBL, which is closely related to the poor stratiform cloud scheme, since explicit cloud water/cloud ice is not prognostic in the FFSL scheme. In fact, the missing microphysical process to form cloud water/ice, such as deposition, sedimentation, melting etc. (Lohmann and Roeckner, 1996), led to the exaggerated biases in water vapor.

The simulated temperature (Figs. 7e and h) of the model was quite similar to that of the reanalysis (Fig. 7b). The positive difference mainly occurred in the lower troposphere, especially at the high latitudes of the Northern Hemisphere. Near the middle troposphere at high latitudes in the Southern Hemisphere, both simulations showed a weak negative difference.

Below the PBL, the dry bias in specific humidity along with warm bias in temperature led to a negative bias in relative humidity (Figs. 7f and i). The reduced bias in FFSL simulation can be mainly attributed to the improved simulation of the water vapor advection process, as the impact of water phase change was negligible below the PBL. Above the PBL, the moist bias led to an increase in relative humidity.

The simulated seasonal averages of specific humidity, temperature, and relative humidity for June–August are shown in Fig. 8. Similar to the winter simulations, both schemes yielded a dry bias in the lower troposphere, along with a moist bias in the upper troposphere (Figs. 8d and g), which was also reflected in relative humidity (Figs. 8f and i). Again, the dry bias below the PBL was effectively reduced in the FFSL simulation, although the moist bias above the PBL

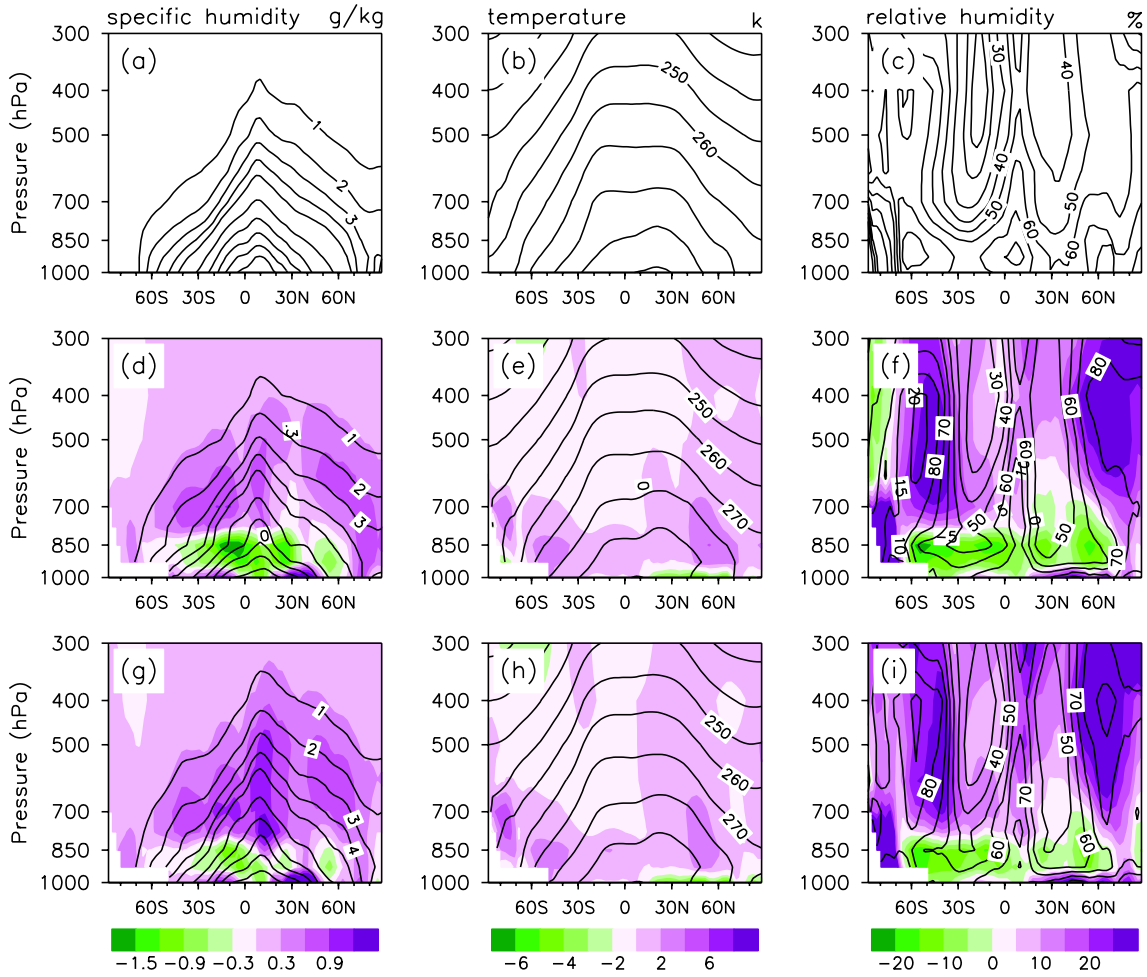

Fig. 8. Same as Fig.7, but for June–August (JJA) averages.

was magnified. However, the temperature bias was somewhat different than the DJF simulations, with the warm bias spreading to a higher altitude. The cold bias near the middle troposphere at high latitudes in the Southern Hemisphere in DJF simulations was replaced by a moderate warm bias. Figure 9 shows the simulated annual-mean precipitable water, together with NCEP/NCAR and ERA40 reanalysis data as a reference. The differences between the model simulations and the ERA40 reanalysis are also presented in Figs. 9c and d (shaded areas). Both sets of reanalysis data revealed a moisture belt along the ITCZ, with major centers located over the oceans. Comparatively, the ERA40 reanalysis showed more precipitable water than the NCEP/NCAR reanalysis. As shown in Figs. 9c and d, both simulations reproduced the observed moisture centers along the ITCZ quite well. However, the water content in both simulations was over-simulated, especially in the FFSL simulation. The overestimation of precipitable water in the FFSL simulation was mainly caused by the increased specific humidity above the PBL, which confirms our previous analysis.

3.2.3 *Large-scale circulation fields*

To quantitatively reveal the similarity between the observed and simulated fields, a Taylor diagram (Taylor, 2001) was created (Fig. 10), with the ERA40 reanalysis data as a reference. For winter, the obtained correlation coefficient was higher with the FFSL scheme. For low-level relative humidity, the correlation coefficient exceeded 70% for the FFSL simulation and was <50% for the SCM simulation. Moreover, the standard deviation was ∼1.0 for the FFSL simulation and ∼1.2 for the SCM simulation. In summer, the general performance of the FFSL scheme was also better than that of the SCM scheme, as reflected by relative humidity levels as well as specific humidity levels. For either winter or summer, the large-scale dynamic field, namely the 200-hPa zonal wind field and the 500-hPa geopotential height, appears to be insensitive to the water vapor advection scheme: both correlation coef-

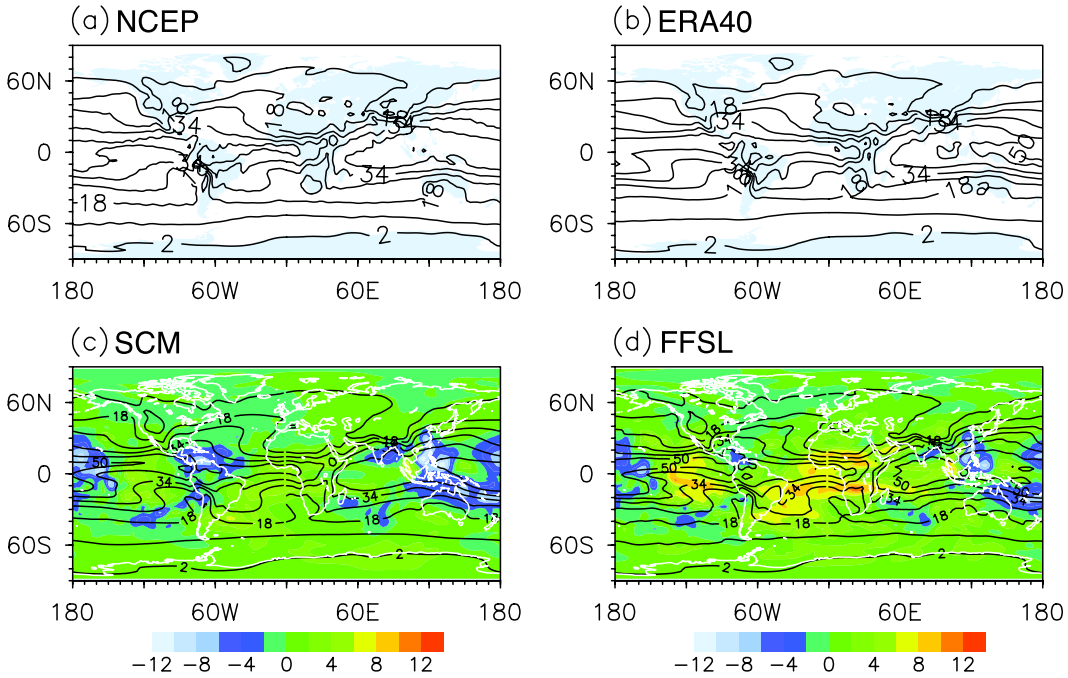

Fig. 9. Horizontal distribution of precipitable water from (a) NCEP/NCAR reanalysis, (b) ERA40 reanalysis, (c) SCM simulation, and (d) FFSL simulation (Units: mm). Differences for simulation minus the ERA40 reanalysis (shaded) are also plotted.

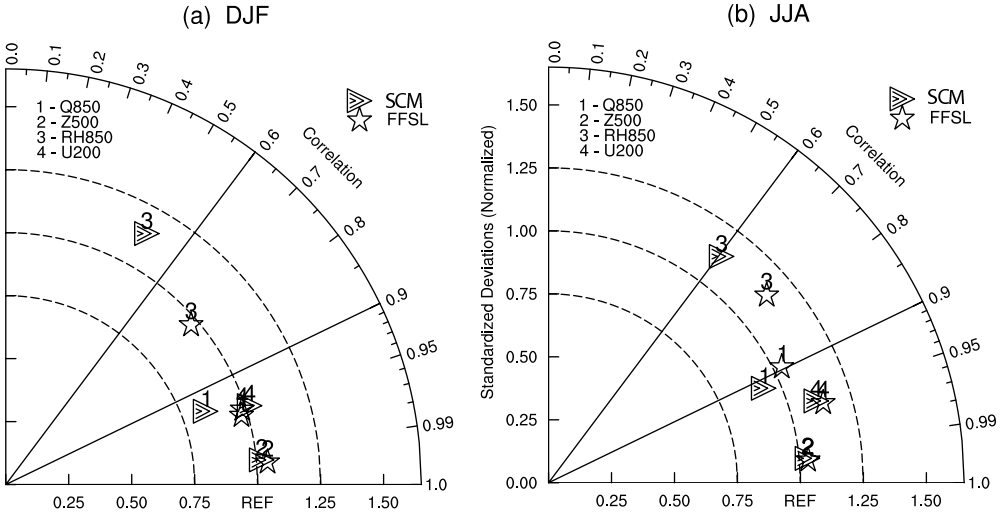

Fig. 10. Correlations between ERA40 reanalysis and simulations for (a) winter and (b) summer.

ficient and standard deviation changed little with the FFSL scheme.

4. Discussion and conclusion

In this study, the PPM-based flux-form semi-Lagrangian transport scheme was implemented in a spectral GCM. Numerical properties such as shape preserving, dispersion accuracy, and oscillation were investigated using a 1D square-wave experiment and an idealized over-polar advection experiment. The negative vapor problem in the previous spectral composition method was eliminated with the FFSL scheme. In the 25-year Atmospheric Model Intercomparison Project (AMIP)-type run, the SCM and FFSL schemes were used as advection schemes for water vapor transport, respectively. Improvements in precipitation distribution as well as precipitation frequency

were observed over the tropics with the FFSL scheme. The FFSL simulation of the seasonal average of zonal means of low-level specific humidity showed a better agreement with the ERA40 reanalysis, but no improvement occurred in the middle and upper troposphere. A Taylor diagram indicated particularly significant correlations between the FFSL simulation and the ERA40 reanalysis data in specific humidity and relative humidity.

The overall performance of the new SAMIL equipped with an FFSL transport scheme showed significant improvement over the old SCM scheme, but the dry bias below the PBL as well as the moist bias above the PBL remained. As is well known, in addition to dynamical transport, physical processes such as PBL turbulence, cumulus convection, cloud formation and dissipation are also important for the hydrologic cycle. Therefore, to further develop SAMIL's performance, more attention should be given to the improvement of physical parameterization schemes, especially the stratiform cloud scheme. Owning to the newly implemented FFSL scheme, the introduction of a prognostic cloud microphysical scheme now seems feasible, as the previous SCM was unsuitable for the advection of discontinuous cloud water/ice. We expect the scheme for the representation of stratiform clouds (consisting of prognostic equations for the vapor, liquid, and ice phase) to further improve the performance of the model. The modification and performance of this improved model will be described and discussed in a future paper.

Acknowledgements. This study was jointly supported by the Chinese Academy of Science Strategic Priority Research Program (Grant No. XDA 05110303), "973" Program (Grant Nos. 2010CB950403, 2012CB417203, and 2013CB955803), "863" Program (Grant No. 2010AA012305), and the National Natural Science Foundation of China (Grant Nos. 40925015, 40875034, and 41023002).

REFERENCES

Adler, R., and Coauthors, 2003: The Version-2 Global Precipitation Climatology Project (GPCP) monthly precipitation analysis (1979–present). *J. Hydrometeor.*, **4**, 1147–1167.

Bao, Q., Y. Liu, T. Zhou, Z. Wang, G. Wu, and P. Wang, 2006: The sensitivity of the spectral atmospheric general circulation model of LASG/IAP to the land process. *Chinese J. Atmos. Sci.*, **30**, 1077–1090. (in Chinese)

Bao, Q., G. Wu, Y. Liu, J. Yang, Z. Wang, and T. Zhou, 2010: An introduction to the coupled model FGOALS1.1-s and its performance in East Asia. *Adv. Atmos. Sci.*, **27**(5), 1131–1142, doi: 10.1007/s00376-010-9177-1.

Colella, P., and P. Woodward, 1984: The piecewise parabolic method (PPM) for gas-dynamical simulations. *J. Comput. Phys.*, **54**, 174–201.

Edwards, J., and A. Slingo, 1996: Studies with a flexible new radiation code. I: Choosing a configuration for a large-scale model. *Quart. J. Roy. Meteor. Soc.*, **122**, 689–720.

Holtslag, A., and B. Boville, 1993: Local versus nonlocal boundary-layer diffusion in a global climate model. *J. Climate*, **6**, 1825–1842.

Kalnay, E, and Coauthors, 1996: The NCEP/ NCAR 40-year reanalysis project. *Bull. Amer. Meteor. Soc.*, **77**, 437–471.

Lin, S., 2004: A "vertically-Lagrangian" finite-volume dynamical core for global atmospheric models. *Mon. Wea. Rev.*, **132**, 2293–2307.

Lin, S., and R. Rood, 1996: Multidimensional flux-form semi-Lagrangian transport scheme. *Mon. Wea. Rev.*, **124**, 2046–2070.

Liu, P., B. Wang, R. K. Sperber, T. Li, and G. A. Meehl, 2005: MJO in the NCAR CAM2 with the Tiedtke Convective Scheme. *J. Climate*, **18**, 3007–3020.

Lohmann, U., and E. Roeckner, 1996: Design and performance of a new cloud microphysics scheme developed for the ECHAM general circulation model. *Climate Dyn.*, **12**, 557–572.

Manabe, S., J. Smagorinsky, and R. Strickler, 1965: Simulated climatology of a general circulation model with a hydrologic cycle. *Mon. Wea. Rev.*, **93**, 769–798.

McDonald, A., 1984: Accuracy of multiply-upstream, semi-Lagrangian advection schemes. *Mon. Wea. Rev.*, **112**, 1267–1275.

McDonald, A., 1987: Accuracy of multiply-upstream, semi-Lagrangian advection schemes II. *Mon. Wea. Rev.*, **115**, 1446–1450.

Nielsen, W. A., 1959: On the application of trajectory methods in numerical forecasting. *Tellus*, **11**, 180–196.

Nordeng, T.-E., 1994: Extended versions of the convective parameterization scheme at ECMWF and their impact on the mean and transient activity of the model in the tropics. Technical Memorandum, No. 206, ECMWF, Shinfield Park, Reading RG 29AX, U.K., 44pp.

Peng, X., F. Xiao, W. Ohfuchi, and H. Fuchigami, 2005: Conservative semi-Lagrangian transport on a sphere and the impact on vapor advection in an atmospheric general circulation model. *Mon. Wea. Rev.*, **133**(3), 504–520.

Ritchie, H., 1985: Application of a semi-Lagrangian integration scheme to the moisture equation in a regional forecast model. *Mon. Wea. Rev.*, **113**, 424–435.

Ritchie, H., 1987: Semi-Lagrangian advection on a Gaussian grid. *Mon. Wea. Rev.*, **115**, 608–619.

Robert, A., 1981: A stable numerical integration scheme for the primitive meteorological equation. *Atmos.-Ocean*, **19**, 35–46.

Robert, A., 1982: Semi-Lagrangian and semi-implicit numerical integration scheme for the primitive meteorological equation. *Quart. J. Roy. Meteor. Soc.*, **60**, 319–324.

Roeckner, E., and Coauthors, 2003: The atmospheric general circulation model ECHAM5. Part I: Model description. Tech. Rep., Max-Planck-Institute, Hamburg, Germany, 127pp.

Rood, R., 1987: Numerical advection algorithms and their role in atmospheric transport and chemistry models. *Rev. Geophys.*, **25**, 71–100.

Slingo, J., 1980: A cloud parameterization scheme derived from GATE data for use with a numerical model. *Quart. J. Roy. Meteor. Soc.*, **106**, 747–770.

Smolarkiewicz, P. K., and W. W. Grabowski, 1990: The multidimensional positive definite advection transport algorithm: Non-oscillatory option. *J. Comput. Phys.*, **86**, 355–375.

Song, X., 2005: The evaluation analysis of two kinds of mass flux cumulus parameterizations in climate simulation. Ph. D. dissertation, Institute of Atmospheric Physics, Chinese Academy of Sciences, Beijing, 156pp. (in Chinese)

Staniforth, A., and J. Côté, 1991: Semi-Lagrangian integration schemes for atmospheric models—A review. *Mon. Wea. Rev.*, **119**, 2206–2223.

Sun, Z., 2005: Parameterizations of radiation and cloud optical properties. BMRC Research Report, 107–112.

Taylor, K., 2001: Summarizing multiple aspect s of model performance in a single diagram. *J. Geophys. Res.*, **106**, 7183–7192.

Tiedtke, M., 1989: A comprehensive mass flux scheme for cumulus parameterization in large-scale models. *Mon. Wea. Rev.*, **117**, 1779–1800.

Uppala, S., and Coauthors, 2005: The ERA-40 reanalysis. *Quart. J. Roy. Meteor. Soc.*, **131**, 2961–3012.

van Leer, B., 1977: Toward the ultimate conservative difference scheme. Part IV: A new approach to numerical convection. *J. Comput. Phys.*, **23**, 276–299.

van Leer, B., 1979: Toward the ultimate conservative difference scheme. Part V: A second order sequel to Godunov's method. *J. Comput. Phys.*, **32**, 101–136.

Wang, X., Q. Bao, K. Liu, G. Wu, and Y. Liu, 2011: Features of rainfall and latent heating structure simulated by two convective parameterization schemes. *Science in China* (*D*), **54**, 1779–1788.

Wang, Z., and Coauthors, 2005a: The development of GOALS/LASGAGCM and its global climatological features in climate simulation I: Influence of horizontal resolution. *Journal of Tropical Meteorology*, **21**, 225–237. (in Chinese)

Wang, Z., and Coauthors, 2005b: The development of GOALS/LASG AGCM and its global climatological features in climate simulation. II: The increase of vertical resolution and its influences. *Journal of Tropical Meteorology*, **21**, 238–247. (in Chinese)

Williamson, D., J. Drake, J. Hack, R. Jackob, and P. Swarztrauber, 1992: A standard test for numerical approximations to the shallow water equations in spherical geometry. *J. Comput. Phys.*, **102**, 211–224.

Wu, G., H. Liu, Y. Zhao, and W. Li, 1996: A nine-layer atmospheric general circulation model and its performance. *Adv. Atmos. Sci.*, **13**(1), 1–18.

Wu, T., Z. Wang, Y. Liu, R. Yu, and G. Wu, 2004: An evaluation of the effects of cloud parameterization in the R42L9 GCM. *Adv. Atmos. Sci.*, **21**, 153–162.

Xiao, F., and X. Peng, 2004: A convexity preserving scheme for conservative advection transport. *J. Comput. Phys.*, **198**, 389–402.

Xiao, F., T. Yabe, X. Peng, and H. Kobayashi, 2002: Conservative and oscillation-less atmospheric transport schemes based on rational functions. *J. Geophys. Res.*, **107**, 4609, doi: 10.1029/2001JD001532.

Yu, R., 1994: A two-step shape-preserving advection scheme. *Adv. Atmos. Sci.*, **11**, 79–90.